AXISYMMETRIC ELASTODYNAMIC RESPONSE FROM NORMAL AND RADIAL IMPACT OF LAYERED COMPOSITES WITH EMBEDDED PENNY-SHAPED CRACKS

G. C. SIH

Institute of Fracture and Solid Mechanics. Lehigh University, Bethlehem, PA 18015, U.S.A.

and

E. P. CHEN †

Sandia Laboratories, Albuquerque, NM 87115, U.S.A.

Abstract—A method is developed for the dynamic stress analysis of a layered composite containing an embedded penny-shaped crack and subjected to normal and radial impact. Quantitatively, the time-dependent stresses near the crack border can be described by the dynamic stress intensity factors. Their magnitude depends on time. on the material properties of the composite and on the relative size of the crack compared to the composite local geometry. Results obtained show that, for the same material properties and geometry of the composite, the dynamic stress intensity factors for an embedded (penny-shaped) crack reach their peak values within a shorter period of time and with a lower magnitude than the corresponding dynamic stress factors for a through-crack.

INTRODUCTION

Advanced composite materials are multi-phased nonhomogeneous materials with anisotropic properties. This complicates the stress analysis for fracture, particularly if the loading is time-dependent, because the crack geometry involves sharp edges.

An effective approach for finding dynamic stresses in a nonhomogeneous composite containing a through crack has been developed [1] by utilizing both the Laplace and Fourier transforms. The transient boundary, symmetry and continuity conditions were formulated by integral representations in terms of the rectangular Cartesian coordinates x and y and the results for the stress intensity factors determined numerically by solving a standard integral equation in the Laplace transform plane. The crack geometry was assumed to extend infinitely in the z-direction or through the side wall of the composite specimen. Many of the failures in fibrous composites, however, were observed [2] to initiate from embedded mechanical imperfections such as air bubbles, voids or cavities. Hence, a more realistic modeling of the actual flaw geometry would be an embedded crack that has finite dimensions in all directions. This immediately suggests a three-dimensional elastodynamic crack problem which cannot be solved effectively by analytical means unless symmetry prevails. One approach for obtaining a solution is to extend the integral transform formulation for a through crack in rectangular coordinates [1] to that of an embedded crack in cylindrical polar coordinates. This necessitates the use of Hankel transforms instead of Fourier transforms.

Although no attempt will be made to analyze the failure of the composite due to impact, the dynamic stress intensity factors $k_1(t)$ and $k_2(t)$ can be readily used in a given fracture criterion, say the strain energy density theory [3], for determining the allowable level of impact load. The new results can therefore assist the construction of composite materials for establishing impact tolerance. In this case, failure is assumed to initiate from a damage zone of material in the composite that can be approximated by an embedded crack. The time-dependent characteristics of the stresses for the through and embedded crack geometries are compared and studied for different elastic properties and dimensions of the composite. In particular, the phenomenon of elastic waves reflecting from the crack to the interfaces within the composite can be exhibited

---

numerically when their neighboring boundaries are sufficiently close to one another. As time becomes very large, all of the results in this report reduce to the corresponding static solutions [4].

AXIAL SYMMETRIC DEFORMATION: PENNY-SHAPED CRACK

Consider a penny-shaped crack of radius a that lies in a layer of material of thickness $2b$ with material properties μ_1, ν_1, ρ_1. This layer is bonded between two media with properties μ_2, ν_2, ρ_2 as illustrated in Fig. 1. With reference to the system of coordinates (x,y,z), the z-axis coincides with the center of the crack and is normal to the crack situated in the xy-plane. The outer boundaries of the composite are assumed to be sufficiently far away from the crack such that the reflected waves will have a negligible influence on the local stresses. Only those impact loads that produce an axisymmetric wave pattern will be considered.

For an axially symmetric deformation field, material elements are displaced only in the radial and axial direction and remain unchanged in the θ-direction. With reference to the cylindrical polar coordinates (r,θ,z) in Fig. 1, the two nonzero displacement components can be expressed in terms of the wave potentials $\phi_j(r,z,t)$ and $\psi_j(r,z,t)$ as follows:

$$(u_r)_j = \frac{\partial \phi_j}{\partial r} - \frac{\partial \psi_j}{\partial z}$$

$$(u_z)_j = \frac{\partial \phi_j}{\partial z} + \frac{\partial \psi_j}{\partial r} - \frac{\psi_j}{r} \tag{1}$$

where $j = 1$ refers to the layer with the crack and $j = 2$ to the surrounding material. The four nontrivial stress components are given by

$$(\sigma_r)_j = 2\mu_j \frac{\partial}{\partial r}\left(\frac{\partial \phi_j}{\partial r} - \frac{\partial \psi_j}{\partial z}\right) + \lambda_j \nabla^2 \phi_j$$

$$(\sigma_\theta)_j = 2\mu_j \frac{1}{r}\left(\frac{\partial \phi_j}{\partial r} - \frac{\partial \psi_j}{\partial z}\right) + \lambda_j \nabla^2 \phi_j$$

$$(\sigma_z)_j = 2\mu_j \frac{\partial}{\partial z}\left(\frac{\partial \phi_j}{\partial z} + \frac{\partial \psi_j}{\partial r} + \frac{\psi_j}{r}\right) + \lambda_j \nabla^2 \phi_j \tag{2}$$

$$(\tau_{rz})_j = \mu_j \left[\frac{\partial}{\partial z}\left(2\frac{\partial \phi_j}{\partial r} - \frac{\partial \psi_j}{\partial z}\right) + \frac{\partial}{\partial r}\left(\frac{\partial \phi_j}{\partial r} + \frac{\psi_j}{r}\right)\right]$$

in which λ_j and μ_j are the Lamé constants and ∇^2 represents the operator

$$\nabla^2 = \frac{\partial^2}{\partial r^2} + \frac{1}{r}\frac{\partial}{\partial r} + \frac{\partial^2}{\partial z^2}.$$

The governing equations can thus be obtained from the equations of motion which yield

$$\frac{\partial^2 \phi_j}{\partial r^2} + \frac{1}{r}\frac{\partial \phi_j}{\partial r} + \frac{\partial^2 \phi_j}{\partial z^2} = \frac{1}{c_{1j}^2}\frac{\partial^3 \phi_j}{\partial t^2}$$

$$\frac{\partial^2 \psi_j}{\partial r^2} + \frac{1}{r}\frac{\partial \psi_j}{\partial r} - \frac{\psi_j}{r^2} + \frac{\partial^2 \psi_j}{\partial z^2} = \frac{1}{c_{2j}^2}\frac{\partial^2 \psi_j}{\partial t^2} \tag{3}$$

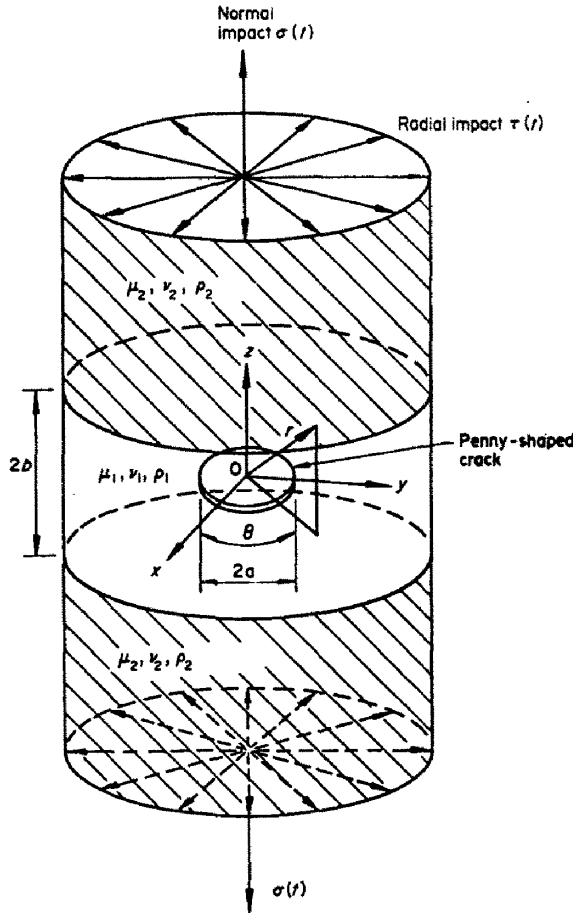with c_{1j} and c_{2j} being the dilatational and shear wave speeds:

Fig. 1. Penny-shaped crack embedded in a matrix layer under normal and radial impact.

$$c_{1j} = \left(\frac{\lambda_j + 2\mu_j}{\rho_j}\right)^{1/2}, \qquad c_{2j} = \left(\frac{\mu_j}{\rho_j}\right)^{1/2}. \tag{4}$$

If the composite body is initially at rest, the Laplace transform of eqns (3) further give

$$\frac{\partial^2 \phi_j^*}{\partial r^2} + \frac{1}{r}\frac{\partial \phi_j^*}{\partial r} + \frac{\partial^2 \phi_j^*}{\partial z^2} = \frac{p^2}{c_{1j}^2}\,\phi_j^*$$

$$\frac{\partial^2 \psi_j^*}{\partial r^2} + \frac{1}{r}\frac{\partial \psi_j^*}{\partial r} - \frac{\psi_j^*}{r^2} + \frac{\partial^2 \psi_j^*}{\partial z^2} = \frac{p^2}{c_{2j}}\,\psi_j^*. \tag{5}$$

Here, p is the transform variable in the Laplace transform pair:

$$f^*(p) = \int_0^\infty f(t) \exp(-pt)\,dt$$

$$f(t) = \frac{1}{2\pi i}\int_{Br} f^*(p) \exp(pt)\,dp. \tag{6}$$

The abbreviation Br stands for the Bromwich path of integration. Moreover, since the composite geometry is symmetrical about the xy-plane, it suffices to consider only the solution in the upper half-space, $z \geq 0$. For the penny-shape crack geometry, the Hankel transform pair

[5] may be used:

$$f^h(s) = \int_0^\infty x f(x) J_n(sx)\, dx$$

(7)

$$f(x) = \int_0^\infty s f^h(s) J_n(sx)\, ds$$

where J_n is the nth order Bessel function of the first kind applying eqns (7) to (5), the following results are obtained:

$$\phi_1^*(r,z,p) = \int_0^\infty [A^{(1)}(s,p) e^{-\gamma_{11} z} + A^{(2)}(s,p) e^{\gamma_{11} z}] J_0(rs)\, ds$$

(8)

$$\psi_1^*(r,z,p) = \int_0^\infty [B^{(1)}(s,p) e^{-\gamma_{21} z} + B^{(2)}(s,p) e^{\gamma_{21} z}] J_1(rs)\, ds$$

for the cracked layer and

$$\phi_2^*(r,z,p) = \int_0^\infty C^{(1)}(s,p) e^{-\gamma_{12} z} J_0(rs)\, ds$$

(9)

$$\psi_2^*(r,z,p) = \int_0^\infty C^{(2)}(s,p) e^{-\gamma_{22} z} J_1(rs)\, ds$$

for the surrounding material. The quantities γ_{ij} are given by

$$\gamma_{1j} = \left(s^2 + \frac{p^2}{c_{1j}^2}\right)^{1/2}, \ \gamma_{2j} = \left(s^2 + \frac{p^2}{c_{2j}^2}\right)^{1/2}.$$

(10)

The six unknowns $A^{(1)}, A^{(2)}, \ldots, C^{(2)}$ are determined from a given set of transient boundary, symmetry and continuity conditions.

NORMAL IMPACT

Let the penny-shaped crack be subjected to a uniform impact load† such that the upper and lower surface will move in the opposite direction. The magnitude of this normal load is σ_0 and, since it is applied suddenly from $t = 0$ and maintained at a constant value thereafter, the Heaviside unit step function, $H(t)$, will be used, i.e. $-\sigma_0 H(t)$. Making use of eqns (6), the conditions on the plane $z = 0$ for $r \le a$ and $r \ge a$ take the forms

$$(\sigma_z^*)_1 (r,o,p) = -\frac{\sigma_0}{p}; (\tau_{rz}^*)_1 (r,o,p) = 0, 0 \le r < a$$

(11)

$$(u_z^*)_1 (r,o,p) = 0; (\tau_{rz}^*)_1 (r,o,p) = 0, r \ge a.$$

If the interfaces at $z = \pm b$ are bonded perfectly, the stresses and displacements can then be

---

†There is no loss in generality in formulating the problem in terms of a uniform step load. The principle of superposition may be used to obtain the solution for general loading from a series of step loading solutions as discussed in [1].

considered to be continuous across these planes, i.e.

$$(\sigma_z^*)_1 (r,b,p) = (\sigma_z^*)_2(r,b,p)$$

$$(\tau_{rz}^*)_1 (r,b,p) = (\tau_{rz}^*)_2 (r,b,p)$$

(12)

and

$$(u_r^*)_1 (r,b,p) = (u_r^*)_2 (r,b,p)$$

$$(u_z^*)_1 (r,b,p) = (u_z^*)_2 (r,b,p).$$

(13)

Under these considerations, the six functions $A^{(1)}$, $A^{(2)}$,..., $C^{(2)}$ may be expressed in terms of a single unknown $A(s,p)$ as indicated by eqns (A1) in the Appendix.

Fredholm integral equations.
Without going into detail, the function $A(s,p)$ can be obtained from the system of dual integral equations

$$\int_0^\infty A(s,p) J_0(rs) \, ds = 0, \, r \geq a$$

(14)

$$\int_0^\infty s P_I(s,p) A(s,p) J_0(rs) \, ds = -\frac{\sigma_0}{2\mu_1 (1-\kappa_1^2)p}, \quad r < a$$

in which $P_I(s,p)$ is a known function:

$$P_I(s,p) = \frac{1}{s\Delta_I(1-\kappa_1^2)} \left\{ \left[\tfrac{1}{4}(s^2 + \gamma_{21}^2)^2 - s^2\gamma_{11}\gamma_{21} \right] [\delta^{(2)} - \delta^{(3)} e^{-2(\gamma_{11}+\gamma_{21})b}] \right.$$
$$+ s(s^2 + \gamma_{21}^2) e^{-(\gamma_{11}+\gamma_{21})b} [\gamma_{21}(\delta^{(1)} \delta^{(4)} - \delta^{(2)} \delta^{(3)}) - \gamma_{11}]$$
$$\left. + [\tfrac{1}{4}(s^2 + \gamma_{21}^2)^2 + s^2\gamma_{11}\gamma_{21}][\delta^{(4)} e^{-2\gamma_{21}b} - \delta^{(1)} e^{-2\gamma_{11}b}] \right\}$$

(15)

The form of $A(s,p)$ that satisfies eqns (14) can be found from Copson [6]:

$$A(s,p) = -\sqrt{\frac{2s}{\pi}} \frac{\sigma_0 a^{5/2}}{2\mu_1 p (1-\kappa_1^2)} \int_0^1 \sqrt{\xi} \, \Lambda_I^*(\xi,p) J_{1/2}(sa\xi) \, d\xi.$$

(16)

Here, $J_{1/2}$ is the half order Bessel function of the first kind and $\Lambda_I^*(\xi,p)$ satisfies the Fredholm integral equation

$$\Lambda_I^*(\xi,p) + \int_0^1 \Lambda_I^*(\eta,p) M_I (\xi,\eta,p) \, d\eta = \xi$$

(17)

whose kernel

$$M_I(\xi,\eta,p) = \sqrt{\xi\eta} \int_0^\infty s \left[P_I\left(\frac{s}{a},p\right) - 1 \right] J_{1/2}(s\xi) J_{1/2}(s\eta) \, ds = \frac{2}{\pi} \int_0^\infty \left[P_I\left(\frac{s}{a},p\right) - 1 \right] \sin(s\xi) \sin(s\eta) \, ds$$

(18)

is symmetric in ξ and η. Figures 2–4 show the numerical results of eqn (17) obtained by varying μ_2/μ_1 and a/b while $\rho_1 = \rho_2$ and $\nu_1 = \nu_2 = 0.29$ are kept the same for all cases. The function $\Lambda_I^*(\xi,p)$ evaluated at the crack border, $\xi = 1$, governs the contribution of the geometric and material parameters on $k_I^*(p)$ which represents the Laplace transform of the stress intensity factor.
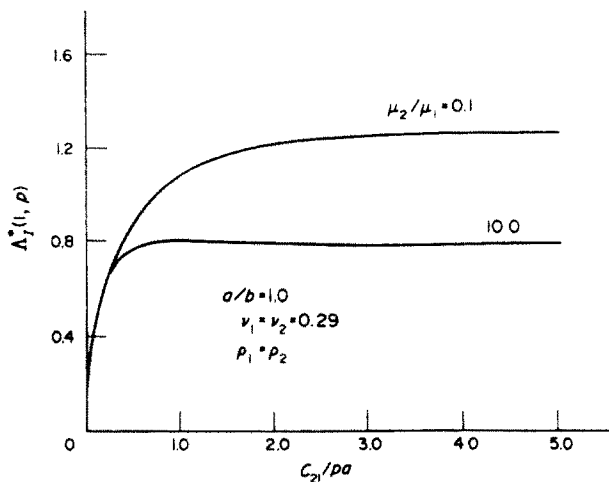
Fig. 2. Plot of $\Lambda_I^*(1,p)$ vs c_{21}/pa for $a/b = 1.0$.

Stress intensity factor for normal impact

In order to evaluate $k_1^*(p)$ or $k_1(t)$, the stresses in the matrix layer are first expanded in terms of the local coordinates r_1 and θ_1 for small values of r_1. The local coordinates (r_1, θ_1) are related to (r, θ) in Fig. 1 as follows:

$$a + r_1 \cos \theta_1 = r \cos \theta$$

$$r_1 \sin \theta_1 = r \sin \theta.$$

(19)

The leading term in the Laplace transform of the local stresses that possess the $1/\sqrt{r_1}$ singularity is

$$k_1^*(p) = \frac{\Lambda_I^*(1,p)}{p} \frac{2}{\pi} \sigma_0 \sqrt{a}.$$

(20)
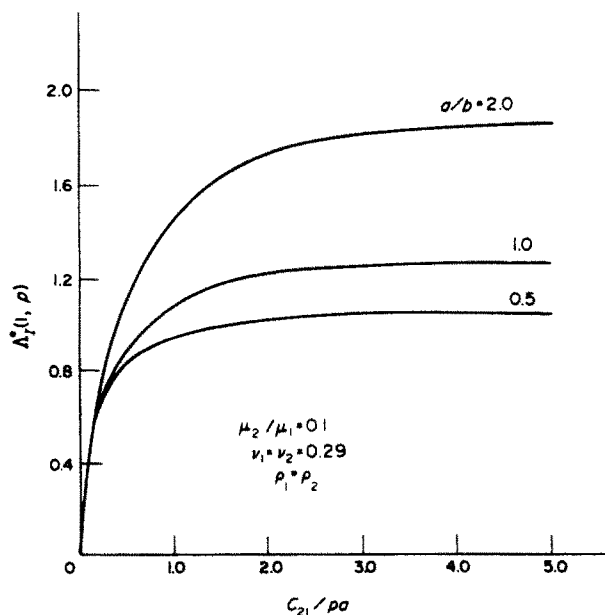
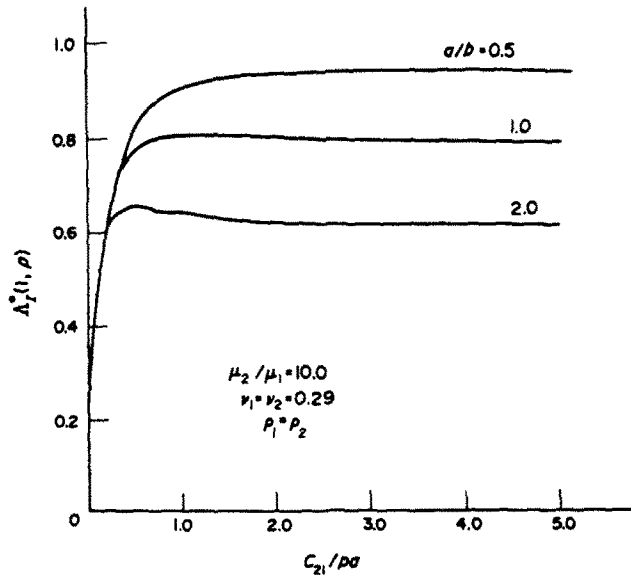Fig. 3. Plot of $\Lambda_I^*(1,p)$ vs c_{21}/pa for $\mu_2/\mu_1 = 0.1$.

Fig. 4. Plot of $\Lambda_I^*(1,p)$ vs c_{21}/pa for $\mu_2/\mu_1 = 10.0$.

Application of the Laplace inversion theorem yields the dynamic stress field around the crack border as a function of time. The result is

$$(\sigma_r)_1 (r_1,\theta_1,t) = \frac{k_1(t)}{\sqrt{2r_1}} \cos\frac{\theta_1}{2}\left(1 - \sin\frac{3\theta_1}{2}\right) + 0(r_1^0)$$

$$(\sigma_\theta)_1 (r_1,\theta_1,t) = \frac{k_1(t)}{\sqrt{2r_1}} 2\nu_1 \cos\frac{\theta_1}{2} + 0(r_1^0)$$

$$(\sigma_z)_1 (r_1,\theta_1,t) = \frac{k_1(t)}{\sqrt{2r_1}} \cos\frac{\theta_1}{2}\left(1 + \sin\frac{\theta_1}{2}\sin\frac{3\theta_1}{2}\right) + 0(r_1^0) \qquad (21)$$

$$(\tau_{rz})_1 (r_1,(\theta_1,t) = \frac{k_1(t)}{\sqrt{2r_1}} \cos\frac{\theta_1}{2}\sin\frac{\theta_1}{2}\cos\frac{3\theta_1}{2} + 0(r_1^0)$$

and $k_1(t)$ becomes

$$k_1(t) = \frac{2\sigma_0\sqrt{a}}{\pi}\frac{1}{2\pi i}\int_{Br} \frac{\Lambda_I^*(1,p)}{p} e^{pt} \,dp. \qquad (22)$$

Note that eqn (20) is, in fact, the Laplace transform of eqn (22). Hence, the functional dependence of r_1 and θ_1 is not affected by the Laplace transformation and can be evaluated separately. This observation was first made by Sih, Ravera and Embley[7].

Making use of the results for $\Lambda_I^*(1,p)$ in Figs. 2–4, $k_1(t)$ in eqn (22) can be found as given in Figs. 5–7. The dynamic stress intensity factors $k_1(t)$ for the penny-shaped crack exhibit an oscillatory behavior rising quickly to a peak. As time increases, all curves will oscillate and eventually approach the static value of $k_1 = 2\sigma_0\sqrt{a}/\pi$ [4]. For a crack diameter to layer thickness ratio of $a/b = 1$, the peaks of the $k_1(t)$ curve are sensitive to changes in the shear moduli ratio μ_2/μ_1. Figure 5 indicates that $k_1(t)$ tends to decrease in amplitude as μ_2/μ_1 is reduced from 0.1 to 10.0. The influence of the composite interface on $k_1(t)$ is exhibited in Figs. 6–7. When the shear modulus of the surrounding material μ_2 is much smaller than the matrix layer with μ_1, the dynamic crack border stress intensity increases as the crack diameter becomes large in comparison with the layer thickness.This effect is clearly evidenced in Fig. 6. As expected, $k_1(t)$ increases with decreasing a/b when the shear modulus of the cracked layer
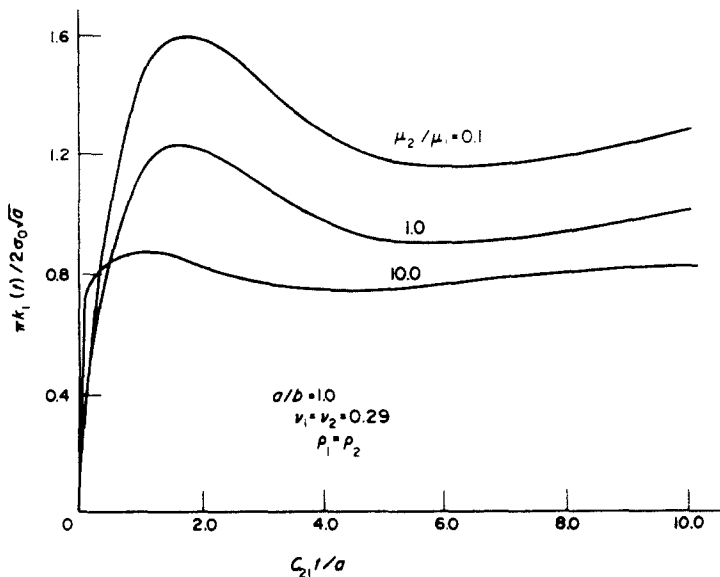
Fig. 5. Dynamic stress intensity factor $k_1(t)$ for penny-shaped crack with $a/b = 1.0$.

is made smaller the surrounding material, i.e. $\mu_1 < \mu_2$ as illustrated in Fig. 7. The results of Embley and Sih [8] is recovered for the homogeneous case, $\mu_1 = \mu_2$.

RADIAL IMPACT

If the penny-shaped crack is sheared uniformly in the radial direction such that axial symmetry is preserved, then $\phi_j^*(r,z,p)$ and $\psi_j^*(r,z,p)$ in eqns (8) and (9) remain valid. Let this shear of magnitude τ_0 be applied suddenly and hence the surface tractions, $-\tau_0 H(t)$, are to be
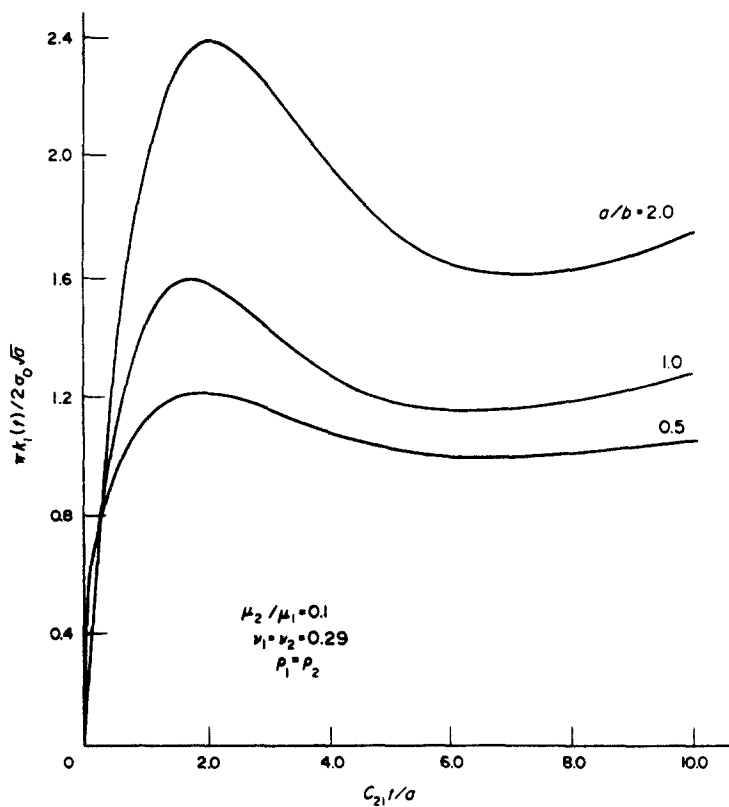

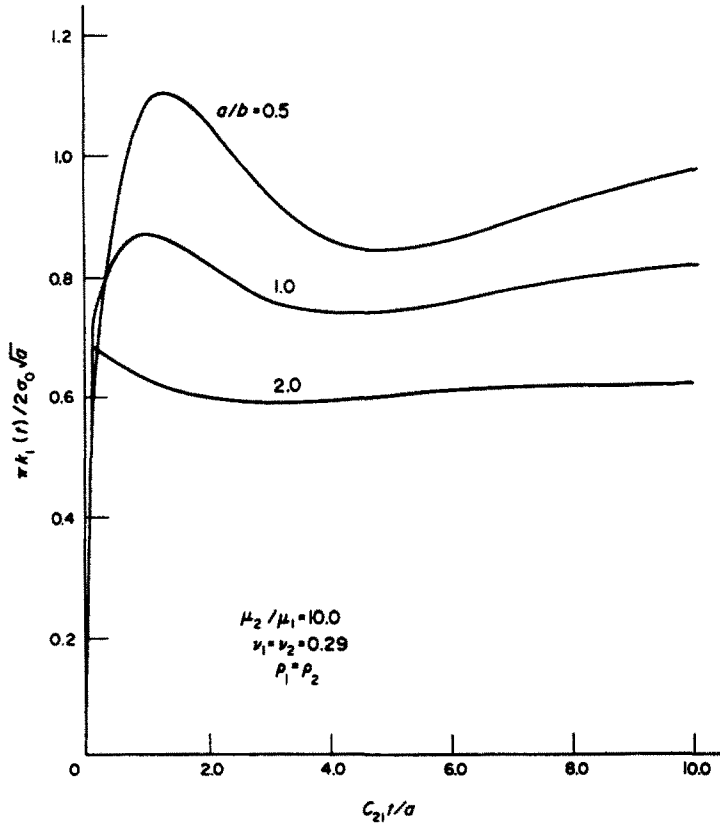Fig. 6. Dynamic stress intensity factor $k_1(t)$ for penny-shaped crack with $\mu_2/\mu_1 = 0.1$.

Fig. 7. Dynamic stress intensity factor $k_1(t)$ for penny-shaped crack with $\mu_2/\mu_1 = 10.0$.

specified for $0 \le r < a$ with $H(t)$ being the Heaviside unit step function. Laplace transform of the conitions on the plane $z = 0$ thus become

$$(\tau_{rz}^*)_1 (r,o,p) = -\frac{\tau_0}{p}; \ (\sigma_z^*)_1 (r,o,p) = 0, \quad 0 \le r < a$$

(23)

$$(u_r^*)_1(r,o,p) = 0; \ (\sigma_z^*)_1(r,o,p) = 0, \quad r \ge a.$$

Continuity of the stresses across the interface $z = b$ is satisfied if

$$(\sigma_z^*)_1 (r,b,p) = (\sigma_z^*)_2 (r,b,p)$$

$$(\sigma_{rz}^*)_1 (r,b,p) = (\sigma_{rz}^*)_2 (r,b,p)$$

(24)

and the same requirement is imposed on the displacements:

$$(u_r^*)_1 (r,b,p) = (u_r^*)_2 (r,b,p)$$

$$(u_z^*)_1 (r,b,p) = (u_z^*)_2 (r,b,p).$$

(25)

Integral equations

As in the case of normal impact, the six unknown functions $A^{(1)}(s,p)$, $A^{(2)}(s,p),\ldots,$ $C^{(2)}(s,p)$ in eqns (8) and (9) can be expressed in terms of a single unknown $B(s,p)$. Refer to eqns (A5) in the Appendix. Hence, eqns (24) and (25) are satisfied. The remaining boundary conditions in eqns (23)

are employed to obtain the system of dual integral equations

$$\int_0^\infty B(s,p) J_1(rs)\, ds = 0, r \geq a$$

(26)

$$\int_0^\infty s P_{II}(s,p) B(s,p) J_1(rs)\, ds = -\frac{\tau_0}{2\mu_1(1-\kappa_1^2)p}, r < a$$

in which

$$P_{II}(s,p) = \frac{\Delta_I}{\Delta_{II}} P_I(s,p)$$

(27)

where $P_I(s,p)$ is already known through eqn (15) while $\Delta_I(s,p)$ and $\Delta_{II}(s,p)$ are given by eqns (A2) and (A6), respectively.

Solving for $B(s,p)$ [6], it can be shown that

$$B(s,p) = -\sqrt{\frac{\pi s}{2}} \frac{\tau_0 a^{5/2}}{4\mu_1 p(1-\kappa_1^2)} \int_0^1 \sqrt{\xi}\, \Lambda_{II}^*(\xi,p) J_{3/2}(sa\xi)\, d\xi$$

(28)

and $\Lambda_{II}^*(\xi,p)$ satisfies the Fredholm integral equation of the second kind:

$$\Lambda_{II}^*(\xi,p) + \int_0^1 \Lambda_{II}^*(\eta,p) M_{II}(\xi,\eta,p)\, d\eta = \xi$$

(29)

whose kernel takes the form

$$M_{II}(\xi,\eta,p) = \sqrt{\xi\eta} \int_0^\infty s\left[P_{II}\left(\frac{s}{a},p\right) - 1 \right] J_{3/2}(s\xi) J_{3/2}(s\eta)\, ds.$$

(30)

Plots of $\Lambda_{II}^*(1,p)$ as a function of c_{21}/pa are shown in Figs. 8–10 for different values of μ_2/μ_1 and a/h. The curves show that $\Lambda_{II}^*(1,p)$ rises rapidly at first and then levels off.

Stress intensity factor for radial impact

The dynamic crack border stress field corresponding to radial shear can be obtained in the same way and expressed in terms of the coordinates (r_1,θ_1) in eqns (19):

$$(\sigma_r)_1(r_1,\theta_1,t) = \frac{k_2(t)}{\sqrt{2r_1}} \sin\frac{\theta_1}{2}\left(2 + \cos\frac{\theta_1}{2}\cos\frac{3\theta_1}{2}\right) + O(r_1^0)$$

$$(\sigma_\theta)_1(r_1,\theta_1,t) = \frac{k_2(t)}{\sqrt{2r_1}}\, 2\nu_1 \sin\frac{\theta_1}{2} + O(r_1^0)$$

(31)

$$(\sigma_z)_1(r_1,\theta_1,t) = -\frac{k_2(t)}{\sqrt{2r_1}} \sin\frac{\theta_1}{2}\cos\frac{\theta_1}{2}\cos\frac{3\theta_1}{2} + O(r_1^0)$$

$$(\tau_{rz})_1(r_1,\theta_1,t) = \frac{k_2(t)}{\sqrt{2r_1}} \cos\frac{\theta_1}{2}\left(1 - \sin\frac{\theta_1}{2}\sin\frac{3\theta_1}{2}\right) + O(r_1^0).$$

Note that $k_2(t)$ can be evaluated from

$$k_2(t) = \frac{\tau_0(\sqrt{a})}{4\pi i} \int_{Br} \frac{\Lambda_{II}^*(1,p)}{p} e^{pt}\, dp$$

(32)
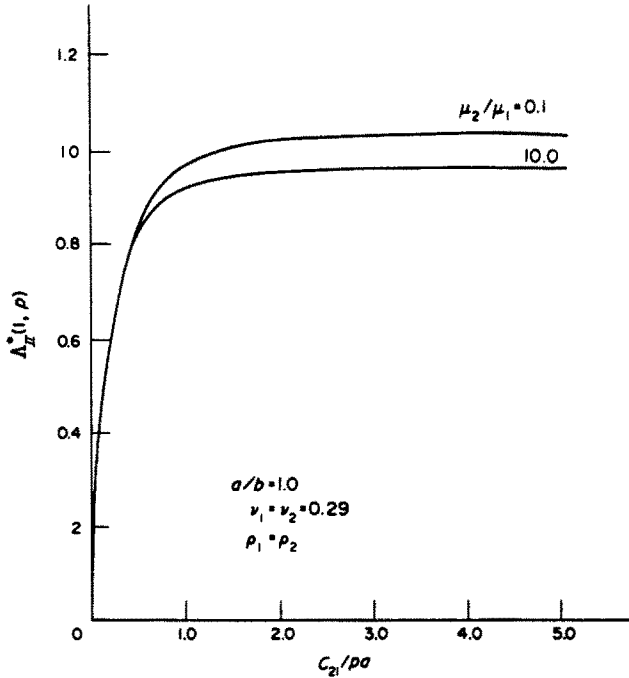
once $\Lambda_{II}^*(1,p)$ as given by Figs. 8–10 is known.

Fig. 8. Variations of $\Lambda_{II}^{*}(1,p)$ with c_{21}/pa for $a/b = 1.0$.

The numerical results in Figs. 11–13 for $k_2(t)$ as a function of time refer to $\rho_1 = \rho_2$ and $\nu_1 = \nu_2 = 0.29$. The curve with $\mu_1 = \mu_2$ is the solution for the homogeneous material treated previously by Embley and Sih [8]. In general, $k_2(t)$ oscillates with time and can be greater or smaller than the corresponding homogeneous solution depending on whether $\mu_2/\mu_1 < 1$ or $\mu_2/\mu_1 > 1$. Figure 11 displays the variations of $k_2(t)$ for different values of μ_2/μ_1 while a/b is fixed at unity. The influence of the ratio of crack size with layer thickness is exhibited in Figs. 12 and 13 for $\mu_2/\mu_1 = 0.1$ and $\mu_2/\mu_1 = 10.0$, respectively. These two cases show the opposite effect which is to be expected.

CONCLUDING REMARKS

The previous discussion has shown that the dynamic stress intensity factors for an embedded crack can be evaluated analytically by a method similar to that developed for a through crack [1]. An important consideration is to compare the results for these two crack configurations and
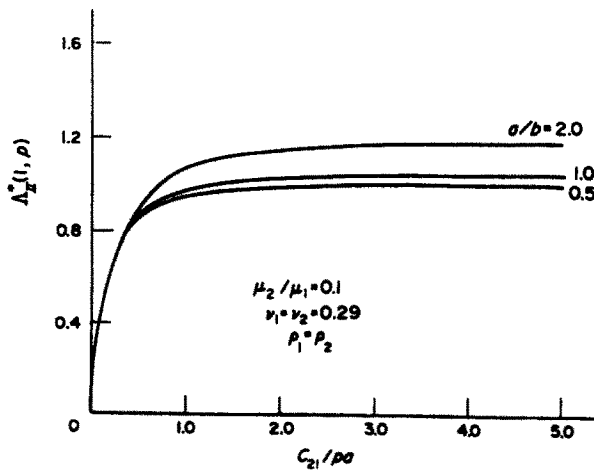

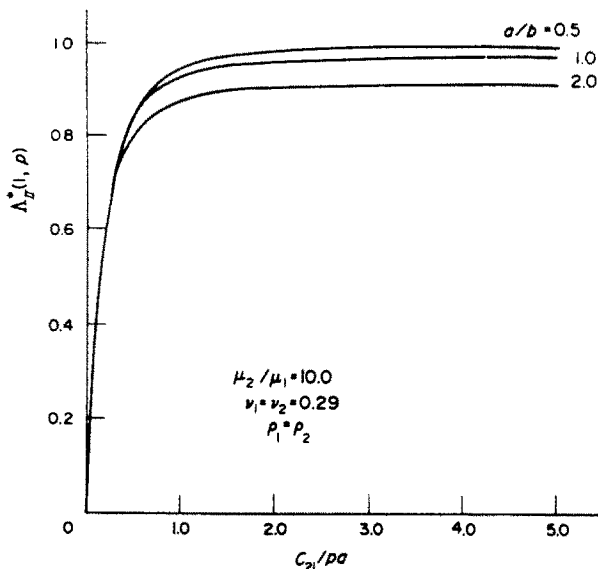Fig. 9. Variations of $\Lambda_{II}^{*}(1,p$ with c_{21}/pa for $\mu_2/\mu_1 = 0.1$ and varying a/b.

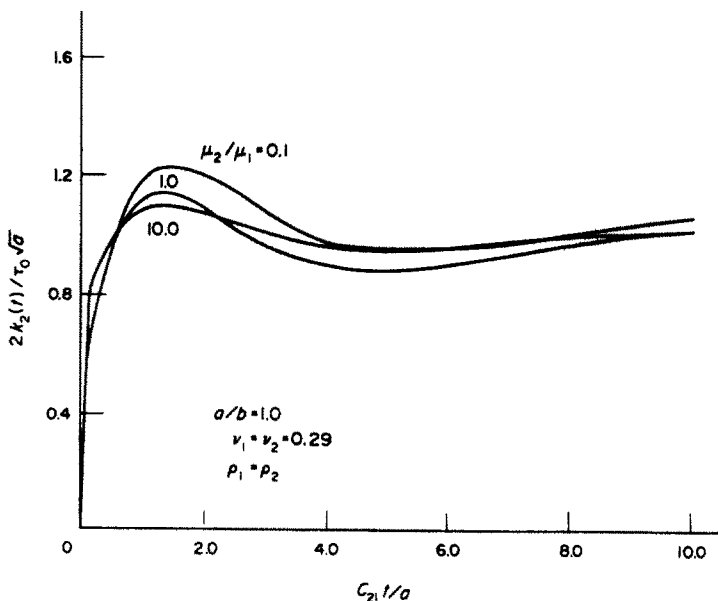Fig. 10. Variations of $\Lambda_I^*(1,p)$ with c_{21}/pa for $\mu_2/\mu_1 = 10$ and varying a/b.

Fig. 11. Stress intensity factor $K_2(t)$ vs time for a penny-shaped crack with $a/b = 1.0$.

to draw some general conclusions. First of all, the $k_1(t)$ or $k_2(t)$ factor for the penny-shaped crack tends to rise more quickly than the through crack, i.e. the peak value of $k_1(t)$ or $k_2(t)$ is reached within a shorter period of time. This is because waves emanating from the neighboring points on the periphery of the penny-shaped crack interfere with each other much earlier as compared to a line (or plane) crack where the waves must travel from one end to the other before interference can take place. In general, the maximum value of $k_1(t)$ or $k_2(t)$ for an embedded crack is lower than that for a through crack. For example, Fig. 5 gives a peak value of approximately 1.6 for $\pi k_1(t)/2\sigma_0\sqrt{a}$ which corresponds to $a/b = 1.0$ and $\mu_2/\mu_1 = 0.1$. This occurs at $c_{21}t/a \simeq 1.6$ and yields $k_1(t) \simeq 1.02\,\sigma_0\sqrt{a}$. The corresponding case of a through crack [1] renders $k_1(t) \simeq 2.40\,\sigma_0\sqrt{a}$ and $c_{21}t/a \simeq 3.0$. The difference in $k_1(t)$ is more than a factor of two and is more pronounced as the ratio a/b is increased. For embedded cracks that are non-circular in shape, approximate estimates of $k_1(t)$ can be made by taking the solution for the
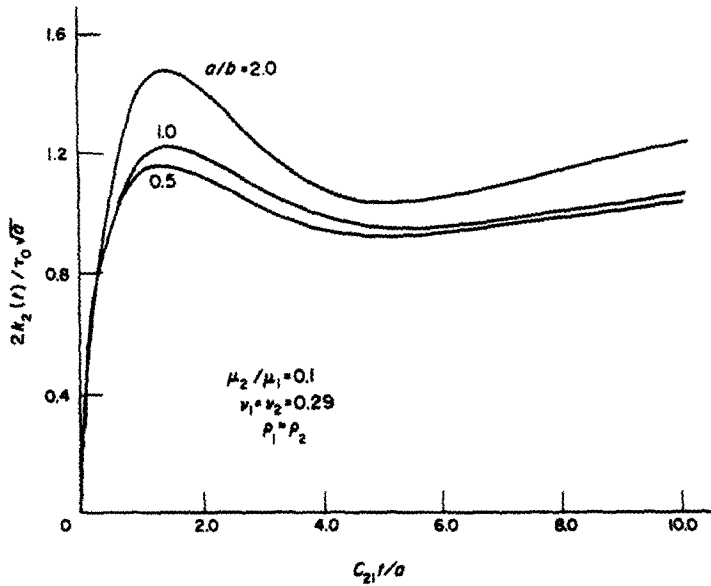
Fig. 12. Stress intensity factor $k_2(t)$ vs time for a penny-shaped crack with $\mu_2/\mu_1 = 0.1$.

through crack as an upper limit and that of the circular crack as a lower limit. Refer to [4] for the case of static loading. It is expected that the same influence of geometry will hold for dynamic loading.

In the absence of axisymmetry, the dynamic stress analysis will become exceedingly difficult and it will be more feasuble to solve the crack problem numerically. In such cases, the solutions obtained here can perhaps be used to guide the development of numerical procedures.
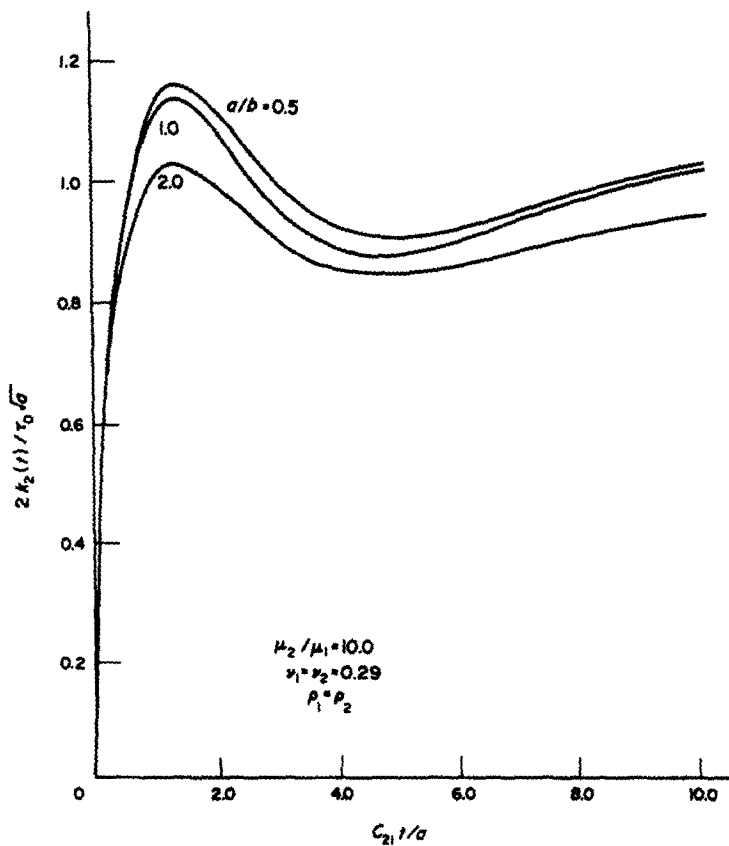

Fig. 13. Stress intensity factor $k_2(t)$ vs time for a penny-shaped crack with $\mu_2/\mu_1 = 10.0$.

REFERENCES

1. G. C. Sih and E. P. Chen, Normal and shear impact of layered composite with a crack: dynamic stress intensification. *J. Appl. Mech.* **47**, 351–358 (1980).
2. K. Lauraitis, Tensile strength of off-axis unidirectional composites. *University of Illinois TAM Report No.* 344 (1971).
3. G. C. Sih, Dynamic crack problems: strain energy density fracture theory. *Mechanics of Fracture*, Vol. IV, pp. XVII–XLVII (Edited by G. C. Sih), Sijthoff and Noordhoff, Alphen (1977).
4. Three-dimensional crack problems. *Mechanics of Fracture*, Vol. II (Edited by G. C. Sih), Sijthoff and Noordhoff, Alphen, Chapter 1 (1975).
5. I. N. Sneddon, *Fourier Transforms.* McGraw-Hill, New York (1958).
6. E. T. Copson, On certain dual integral equations. *Proc. of Glasgow Mathematical Association*, **5**, 19–24 (1961).
7. G. C. Sih, R. S. Ravera and G. T. Embley, Impact response of a finite crack in plane extension. *Int. J. Solids Structures* **8**, 977–993 (1972).
8. G. T. Embley and G. C. Sih, Response of a penny-shaped crack to impact waves. *Proc. of the 12th Midwestern Mechanics Conference*, **6**, 473–487 (1971).

APPENDIX: EXPRESSIONS FOR $A^{(1)}(s,p), \ldots, C^{(1)}(s,p)$

Normal impact

The functions $A^{(1)}(s,p), A^{(2)}(s,p), \ldots, C^{(2)}(s,p)$ for the wave potentials in eqns (8) and (9) can be expressed in terms of a single unknown $A(s,p)$ for normal impact

$$A^{(1)}(s,p) = \left[\tfrac{1}{2}(s^2 + \gamma_{21}^2)(\delta^{(2)} + \delta^{(4)}e^{-2\gamma_{21}b}) - s\gamma_{11}e^{-(\gamma_{11}+\gamma_{21})b}\right]\frac{A(s,p)}{\Delta_t}$$

$$A^{(2)}(s,p) = -\left[s\gamma_{11}e^{-(\gamma_{11}+\gamma_{21})b} + \tfrac{1}{2}(s^2 + \gamma_{21}^2)e^{-2\gamma_{11}b}(\delta^{(1)} + \delta^{(3)}e^{-2\gamma_{21}b})\right]\frac{A(s,p)}{\Delta_t}$$

$$B^{(1)}(s,p) = -\left[\delta^{(1)}A^{(1)}e^{-\gamma_{11}b} + \delta^{(2)}A^{(2)}e^{\gamma_{11}b}\right]$$

$$B^{(2)}(s,p) = -\left[\delta^{(3)}A^{(1)}e^{-\gamma_{11}b} + \delta^{(4)}A^{(2)}e^{\gamma_{11}b}\right] \tag{A1}$$

$$C^{(1)}(s,p) = \frac{e^{\gamma_{12}b}}{s^2 - \gamma_{12}\gamma_{22}}\left[(s^2 - \gamma_{11}\gamma_{22})A^{(1)}e^{-\gamma_{11}b} + (s^2 + \gamma_{11}\gamma_{22})A^{(2)}e^{\gamma_{11}b}\right.$$
$$\left. - s(\gamma_{21} - \gamma_{22})B^{(1)}e^{-\gamma_{21}b} + s(\gamma_{21} + \gamma_{22})B^{(2)}e^{\gamma_{21}b}\right]$$

$$C^{(2)}(s,p) = \frac{e^{\gamma_{22}b}}{s^2 - \gamma_{12}\gamma_{22}}\left[s(\gamma_{12} - \gamma_{11})A^{(1)}e^{-\gamma_{11}b} + s(\gamma_{11} + \gamma_{12})e^{\gamma_{11}b}\right.$$
$$\left. + (s^2 - \gamma_{21}\gamma_{12})B^{(1)}e^{-\gamma_{21}b} + (s^2 + \gamma_{21}\gamma_{12})B^{(2)}e^{\gamma_{21}b}\right]$$

in which Δ_t stands for

$$\Delta_t(s,p) = \frac{p^2}{2c_{21}^2}\gamma_{11}\left[\delta^{(2)} + \delta^{(3)}e^{-2(\gamma_{11}+\gamma_{21})b} + \delta^{(4)}e^{-2\gamma_{21}b} + \delta^{(1)}e^{-2\gamma_{11}b}\right] \tag{A2}$$

and $\delta^{(1)}, \delta^{(2)}, \ldots, \delta^{(4)}$ are further expressed in terms of $e^{(1)}, e^{(2)}, \ldots, e^{(8)}$ as the following:

$$\delta^{(1)}(s,p) = (e^{(1)}e^{(6)} - e^{(2)}e^{(7)})/(e^{(1)}e^{(6)} - e^{(2)}e^{(5)})$$

$$\delta^{(2)}(s,p) = (e^{(4)}e^{(6)} - e^{(2)}e^{(8)})/(e^{(1)}e^{(6)} - e^{(2)}e^{(5)})$$

$$\delta^{(3)}(s,p) = (e^{(1)}e^{(7)} - e^{(3)}e^{(5)})/(e^{(1)}e^{(6)} - e^{(2)}e^{(5)}) \tag{A3}$$

$$\delta^{(4)}(s,p) = (e^{(1)}e^{(8)} - e^{(4)}e^{(5)})/(e^{(1)}e^{(6)} - e^{(2)}e^{(5)}).$$

The quantities in eqns (A3) are complicated functions of the materials parameters and transform variables. They are given by

$$e^{(1)}(s,p) = -s\gamma_{21} + \frac{s\mu_2}{\mu_1(s^2 - \gamma_{12}\gamma_{22})}\left[\tfrac{1}{2}(\gamma_{21} - \gamma_{22})(s^2 + \gamma_{22}^2) + \gamma_{22}(s^2 - \gamma_{21}\gamma_{12})\right]$$

$$e^{(2)}(s,p) = s\gamma_{21} - \frac{s\mu_2}{\mu_1(s^2 - \gamma_{12}\gamma_{22})}\left[\tfrac{1}{2}(\gamma_{21} + \gamma_{22})(s^2 + \gamma_{22}^2) - \gamma_{22}(s^2 + \gamma_{21}\gamma_{12})\right]$$

$$e^{(3)}(s,p) = \tfrac{1}{2}(s^2 + \gamma_{21}^2) - \frac{\mu_2}{\mu_1(s^2 - \gamma_{12}\gamma_{22})}\left[\tfrac{1}{2}(s^2 + \gamma_{22}^2)(s^2 - \gamma_{11}\gamma_{22}) + s^2\gamma_{22}(\gamma_{11} - \gamma_{12})\right]$$

$$e^{(4)}(s,p) = \tfrac{1}{2}(s^2 + \gamma_{21}^2) - \frac{\mu_2}{\mu_1(s^2 - \gamma_{12}\gamma_{22})}\left[\tfrac{1}{2}(s^2 + \gamma_{22}^2)(s^2 + \gamma_{11}\gamma_{22}) - s^2\gamma_{22}(\gamma_{11} + \gamma_{12})\right]$$

$$e^{(5)}(s,p) = -\frac{1}{2}(s^2 + \gamma_{21}^2) + \frac{\mu_2}{\mu_1(s^2 - \gamma_{12}\gamma_{22})}[s^2\gamma_{12}(\gamma_{21} - \gamma_{22}) + \frac{1}{2}(s^2 + \gamma_{22}^2)(s^2 - \gamma_{21}\gamma_{12})]$$

$$e^{(6)}(s,p) = -\frac{1}{2}(s^2 + \gamma_{21}^2) - \frac{\mu_2}{\mu_1(s^2 - \gamma_{12}\gamma_{22})}[s^2\gamma_{12}(\gamma_{21} + \gamma_{22}) - \frac{1}{2}(s^2 + \gamma_{22}^2)(s^2 + \gamma_{21}\gamma_{12})]$$

$$e^{(7)}(s,p) = s\gamma_{11} - \frac{s\mu_2}{\mu_1(s^2 - \gamma_{12}\gamma_{22})}[\gamma_{12}(s^2 - \gamma_{11}\gamma_{22}) + \frac{1}{2}(s^2 + \gamma_{22}^2)(\gamma_{11} - \gamma_{12})] \tag{A4}$$

$$e^{(8)}(s,p) = -s\gamma_{11} - \frac{s\mu_2}{\mu_1(s^2 - \gamma_{12}\gamma_{22})}[\gamma_{12}(s^2 + \gamma_{11}\gamma_{22}) - \frac{1}{2}(s^2 + \gamma_{22}^2)(\gamma_{11} + \gamma_{12})]$$

Radial impact

For radial impact, $A^{(1)}(s,p)$, $A^{(2)}(s,p)$, ..., $C^{(2)}(s,p)$ in eqns (8) and (9) can be expressed in terms of $B(s,p)$ as

$$A^{(1)}(s,p) = -[s\gamma_{21}(\delta^{(2)} - \delta^{(4)}e^{-2\eta_{21}b}) + \frac{1}{2}(s^2 + \gamma_2^2)e^{-(\eta_{11} + \eta_{21})b}]\frac{B(s,p)}{\Delta_{II}}$$

$$A^{(2)}(s,p) = [s\gamma_{21}e^{-2\eta_{11}b}(\delta^{(1)} - \delta^{(3)}e^{2\eta_{21}b}) + \frac{1}{2}(s^2 + \gamma_{21}^2)e^{-(\eta_{11} + \eta_{21})b}]\frac{B(s,p)}{\Delta_{II}} \tag{A5}$$

where

$$\Delta_{II} = \frac{p^2}{2c_{21}^2}\gamma_{21}[\delta^{(2)} + \delta^{(3)}e^{-2(\eta_{11} + \eta_{21})b} - \delta^{(4)}e^{-2\eta_{21}b} - \delta^{(1)}e^{-2\eta_{11}b}]. \tag{A6}$$

The remaining functions $B^{(1)}(s,p)$, $B^{(2)}(s,p)$, etc. can be related to $B(s,p)$ through $A^{(1)}(s,p)$ and $A^{(2)}(s,p)$ since the last four expressions in eqns (A1) for normal impact also apply to radial impact.